Two-photon excited fluorescence in the LYB:Eu monoclinic crystal: towards a new scheme of single-beam dual-voxel direct laser writing in crystals

Yannick Petit, Arnaud Royon, Nicolas Marquestaut, Marc Dussauze, Alexandre Fargues, Philippe Veber, Veronique Jubera, Thierry Cardinal, Lionel Canioni

Two-photon excited fluorescence in the LYB:Eu monoclinic crystal: towards a new scheme of single-beam dual-voxel direct laser writing in crystals

Y. Petit,[1,2,3,4,*] A. Royon,[1,2] N. Marquestaut,[1,2] M. Dussauze,[5,6] A. Fargues,[3,4] P. Veber,[3,4] V. Jubera,[3,4] T. Cardinal,[3,4] and L. Canioni[1,2]

[1]Univ. Bordeaux, LOMA, UMR 5798, F-33400 Talence, France
[2]CNRS, LOMA, UMR 5798, F-33400 Talence, France
[3]CNRS, ICMCB, UPR 9048, F-33608 Pessac, France
[4]Univ. Bordeaux, ICMCB, UPR 9048, F-33400 Pessac, France
[5]Univ. Bordeaux, ISM, UMR 5255, F-33400 Talence, France
[6]CNRS, ISM, UMR 5255, F-33400 Talence, France
[*]yannick.petit@u-bordeaux1.fr

Abstract: We report on two-photon excited fluorescence in the oriented Eu^{3+}-doped LYB monoclinic crystal under femtosecond laser tight focusing. Due to spatial walk-off, the two polarization modes of the incident femtosecond beam simultaneously provide the independent excitation of two distinct focuses, leading to a single-beam dual-voxel nonlinear excitation of fluorescence below material modification threshold. These observations emphasize on the anisotropy of both two-photon absorption as well as fluorescence emission. They demonstrate the localized control of the nonlinear energy deposit, thanks to the adjustment of both the input power and polarization, by properly balancing the injected energy in each voxel. Such approach should be considered for future direct laser writing of waveguides in propagation directions out of the dielectric axes, so as to optimally cope with the highly probable anisotropy of laser-induced material modification thresholds in these crystals. These results open new ways for further potential developments in direct laser writing as the simultaneous inscription of double-line structures for original waveguides processes.

OCIS codes: (160.1190) Anisotropic optical materials; (260.1180) Crystal optics; (260.1440) Birefringence; (270.4180) Multiphoton processes; (300.2530) Fluorescence, laser-induced; (260.5430) Polarization; (230.7370) Waveguides; (050.6875) Three-dimensional fabrication.

References and links

1. R. R. Gattass and E. Mazur, "Femtosecond laser micromachining in transparent materials," Nat. Photonics **2**(4), 219–225 (2008).
2. K. M. Davis, K. Miura, N. Sugimoto, and K. Hirao, "Writing waveguides in glass with a femtosecond laser," Opt. Lett. **21**(21), 1729–1731 (1996).
3. J. Qiu, K. Miura, T. Suzuki, T. Mitsuyu, and K. Hirao, "Permanent photoreduction of Sm^{3+} to Sm^{2+} inside a sodium aluminoborate glass by an infrared femtosecond pulsed laser," Appl. Phys. Lett. **74**(1), 10–12 (1999).
4. A. Royon, K. Bourhis, M. Bellec, G. Papon, B. Bousquet, Y. Deshayes, T. Cardinal, and L. Canioni, "Silver clusters embedded in glass as a perennial high capacity optical recording medium," Adv. Mater. (Deerfield Beach Fla.) **22**(46), 5282–5286 (2010).
5. M. Shimizu, M. Sakakura, M. Ohnishi, Y. Shimotsuma, T. Nakaya, K. Miura, and K. Hirao, "Vortex Dynamics in hcp Solid ^{4}He," J. Appl. Phys. **108**, 073533 (2010).
6. E. Brasselet, A. Royon, and L. Canioni, "Dense arrays of microscopic optical vortex generators from femtosecond direct laser writing of radial birefringence in glass," Appl. Phys. Lett. **100**(18), 181901 (2012).

#175917 - $15.00 USD Received 11 Sep 2012; revised 4 Nov 2012; accepted 4 Nov 2012; published 8 Jan 2013

7. A. Podlipensky, A. Abdolvand, G. Seifert, and H. Graener, "Femtosecond laser assisted production of dichroitic 3D structures in composite glass containing Ag nanoparticles," Appl. Phys., A Mater. Sci. Process. **80**(8), 1647–1652 (2005).
8. Y. Shimotsuma, P. G. Kazansky, J. Qiu, and K. Hirao, "Self-Organized Nanogratings in Glass Irradiated by Ultrashort Light Pulses," Phys. Rev. Lett. **91**(24), 247405 (2003).
9. C. Hnatovsky, R. S. Taylor, E. Simova, V. R. Bhardwaj, D. M. Rayner, and P. B. Corkum, "Polarization-selective etching in femtosecond laser-assisted microfluidic channel fabrication in fused silica," Opt. Lett. **30**(14), 1867–1869 (2005).
10. J. Choi, M. Bellec, A. Royon, K. Bourhis, G. Papon, T. Cardinal, L. Canioni, and M. Richardson, "Three-dimensional direct femtosecond laser writing of second-order nonlinearities in glass," Opt. Lett. **37**(6), 1029–1031 (2012).
11. Y. Dai, B. Zhu, J. Qiu, H. Ma, B. Lu, and B. Yu, "Space-selective precipitation of functional crystals in glass by using a high repetition rate femtosecond laser," Chem. Phys. Lett. **443**(4-6), 253–257 (2007).
12. Y. Liu, B. Zhu, Y. Dai, X. Qiao, S. Ye, Y. Teng, Q. Guo, H. Ma, X. Fan, and J. Qiu, "Femtosecond laser writing of Er^{3+}-doped CaF_2 crystalline patterns in glass," Opt. Lett. **34**(21), 3433–3435 (2009).
13. A. Royon, Y. Petit, G. Papon, M. Richardson, and L. Canioni, "Femtosecond laser induced photochemistry in materials tailored with photosensitive agents," Opt. Mater. Express **1**(5), 866–882 (2011).
14. J. Siebenmorgen, K. Petermann, G. Huber, K. Rademaker, S. Nolte, and A. Tünnermann, "Femtosecond laser written stress-induced Nd:Y3Al5O12 (Nd:YAG) channel waveguide laser," Appl. Phys. B **97**(2), 251–255 (2009).
15. K. Kawamura, M. Hirano, T. Kurobori, D. Takamizu, T. Kamiya, and H. Hosono, "Femtosecond-laser-encoded distributed-feedback color center laser in lithium fluoride single crystals," Appl. Phys. Lett. **84**(3), 311 (2004).
16. V. Apostolopoulos, L. Laversenne, T. Colomb, C. Depeursinge, R. P. Salathé, M. Pollnau, R. Osellame, G. Cerullo, and P. Laporta, "Femtosecond-irradiation-induced refractive-index changes and channel waveguiding in bulk Ti^{3+}:Sapphire," Appl. Phys. Lett. **85**(7), 1122 (2004).
17. F. M. Bain, A. A. Lagatsky, R. R. Thomson, N. D. Psaila, N. V. Kuleshov, A. K. Kar, W. Sibbett, and C. T. A. Brown, "Ultrafast laser inscribed Yb:$KGd(WO_4)_2$ and Yb:$KY(WO_4)_2$ channel waveguide lasers," Opt. Express **17**(25), 22417–22422 (2009).
18. S. M. Eaton, C. A. Merchant, R. Iyer, A. J. Zilkie, A. S. Helmy, J. S. Aitchison, P. R. Herman, D. Kraemer, R. J. D. Miller, C. Hnatovsky, and R. S. Taylor, "Raman gain from waveguides inscribed in $KGd(WO_4)_2$ by high repetition rate femtosecond laser," Appl. Phys. Lett. **92**(8), 081105 (2008).
19. J. Burghoff, C. Grebing, S. Nolte, and A. Tünnermann, "Efficient frequency doubling in femtosecond laser-written waveguides in lithium niobate," Appl. Phys. Lett. **89**(8), 081108 (2006).
20. S. J. Beecher, R. R. Thomson, D. T. Reid, N. D. Psaila, M. Ebrahim-Zadeh, and A. K. Kar, "Strain field manipulation in ultrafast laser inscribed BiB_3O_6 optical waveguides for nonlinear applications," Opt. Lett. **36**(23), 4548–4550 (2011).
21. T. Gorelik, M. Will, S. Nolte, A. Tuennermann, and U. Glatzel, "Transmission electron microscopy studies of femtosecond laser induced modifications in quartz," Appl. Phys., A Mater. Sci. Process. **76**(3), 309–311 (2003).
22. R. R. Thomson, S. Campbell, I. J. Blewett, A. K. Kar, and D. T. Reid, "Optical waveguide fabrication in z-cut lithium niobate (LiNbO3) using femtosecond pulses in the low repetition rate regime," Appl. Phys. Lett. **88**(11), 111109 (2006).
23. W. Yang, P. G. Kazansky, and Y. P. Svirko, "Non-reciprocal ultrafast laser writing," Nature **2**, 99–104 (2008).
24. L. Yang, C. Wang, Y. Dong, N. Da, X. Hu, D. Chen, and J. Qiu, "Three-photon-excited upconversion luminescence of YVO_4 single crystal by infrared femtosecond laser irradiation," Opt. Express **13**(25), 10157–10162 (2005).
25. A. Ródenas, A. H. Nejadmalayeri, D. Jaque, and P. Herman, "Confocal Raman imaging of optical waveguides in $LiNbO_3$ fabricated by ultrafast high-repetition rate laser-writing," Opt. Express **16**(18), 13979–13989 (2008).
26. Y. Petit, B. Boulanger, P. Segonds, C. Félix, B. Ménaert, J. Zaccaro, and G. Aka, "Absorption and fluorescence anisotropies of monoclinic crystals: the case of Nd:YCOB," Opt. Express **16**(11), 7997–8002 (2008).
27. S. Joly, Y. Petit, B. Boulanger, P. Segonds, C. Félix, B. Ménaert, and G. Aka, "Singular topology of optical absorption in biaxial crystals," Opt. Express **17**(22), 19868–19873 (2009).
28. S. Joly, P. Segonds, B. Boulanger, Y. Petit, A. P. Revellez, C. Félix, and B. Ménaert, "Rotation of the absorption frame as a function of the electronic transition in the Nd^{3+}:$YCa_4O(BO_3)_3$ monoclinic crystal," Opt. Express **18**(18), 19169–19174 (2010).
29. J. Hölsa and M. Leskelä, "Optical study of Eu3+ luminescence in lithium rare earth borates, $Li_6RE(BO_3)_3$; RE = Gd, Y," J. Lumin. **48-49**, 497–500 (1991).
30. V. Jubera, J.-P. Chaminade, A. Garcia, F. Guillen, and C. Fouassier, "Luminescent properties of Eu^{3+}-activated lithium rare earth borates and oxyborates," J. Lumin. **101**(1-2), 1–10 (2003).
31. G. K. Abdullaev and K. S. Mamedov, Sov. Phys. Crystallogr. **22**(2), 220–222 (1997).
32. M. Born and E. Wolf, *Principles of Optics* (Oxford, 1965).
33. H. Hellwig, J. Liebertz, and L. Bohaty, "Linear optical properties of the monoclinic bismuth BiB_3O_6," J. Appl. Phys. **88**(1), 240 (2000).
34. P. Segonds, V. Jubera, J. Debray, and B. Ménaert, private communication.
35. B. Boulanger and J. Zyss, *International Tables for Crystallography* Vol. **D**: A. Authier Ed., International Union of Crystallography, (Kluwer, Academic Publisher, 2006), chap. 1.7: nonlinear optical properties.

#175917 - $15.00 USD Received 11 Sep 2012; revised 4 Nov 2012; accepted 4 Nov 2012; published 8 Jan 2013

36. P. Segonds, B. Boulanger, J. P. Fève, B. Ménaert, J. Zaccaro, G. Aka, and D. Pelenc, "Linear and nonlinear optical properties of the monoclinic $Ca_4YO(BO_3)_3$ crystal," J. Opt. Soc. Am. B **21**(4), 765–769 (2004).
37. M. Chavoutier, V. Jubera, P. Veber, M. Velazquez, O. Viraphong, J. Hejtmanek, R. Decourt, J. Debray, B. Menaert, P. Segonds, F. Adamietz, V. Rodriguez, I. Manek-Hönninger, A. Fargues, D. Descamps, and A. Garcia, "Thermal, optical and spectroscopic characterizations of borate laser crystals," J. Solid State Chem. **184**(2), 441–446 (2011).
38. P. Segonds, B. Boulanger, L. Ferrier, B. Ménaert, and J. Zaccaro, "Refractive indices determination of a small-size nonlinear biaxial crystal by use of double-refraction measurements with a laser beam," J. Opt. Soc. Amer. B. **23**(5), 852–856 (2006).
39. R. W. Boyd, *Nonlinear Optics* (Academic Press ELSEVIER, San Diego, 2008).
40. S. Brasselet, V. Le Floc'h, F. Treussart, J.-F. Roch, J. Zyss, E. Botzung-Appert, and A. Ibanez, "In situ diagnostics of the crystalline nature of single organic nanocrystals by nonlinear microscopy," Phys. Rev. Lett. **92**(20), 207401 (2004).
41. Y. Petit, S. Joly, P. Segonds, and B. Boulanger, "Recent advances in monoclinic crystal optics," Laser Phys. Rev.: Invited Review Article (to appear in press).
42. R. Cattoor, I. Manek-Hönninger, J.-Ch. Delagnes, Y. Petit, B. Bousquet, V. Jubera, A. Fargues, Ph. Veber, M. Velazquez, A. Garcia, and L. Canioni, "Potential of the Eu:LYB crystal as a laser material for DPSS lasers emitting at 613 nm," Proc. SPIE **8235**, 82351A, 82351A–7 (2012).
43. J.-P. Fève, B. Boulanger, B. Ménaert, and O. Pacaud, "Continuous tuning of a microlaser-pumped optical parametric generator by use of a cylindrical periodically poled lithium niobate crystal," Opt. Lett. **28**(12), 1028–1030 (2003).
44. Y. Petit, P. Segonds, B. Boulanger, and T. Taira, "Angular Quasi-Phase Matching," Phys. Rev. A **76**(6), 063817 (2007).

1. Introduction

Femtosecond (fs) Direct Laser writing (DLW) has largely developed this last decade, resulting from simultaneous progresses in both fs laser technologies and material sciences, leading to innovative light/matter interactions and subsequent material modifications [1]. DLW has already demonstrated many successful approaches to perform localized three-dimensional (3D) structuring of prepared materials, especially in isotropic material such as glasses, permitting photonic applications such as optical waveguides [2] or perennial high density data storage [3,4]. DLW can lead to isotropic laser-induced response, but also to anisotropic properties such as radial birefringence enabling the generation of optical vortices [5,6], geometrical birefringence related to metal nanoparticle reshaping from spherical to oblate/prolate shapes [7], or polarization-dependent oriented nanocrack structures featuring polarization-dependent gratings [8,9]. DLW can also lead to anisotropic structuring such as the generation of buried static electric fields that lead to effective second-order nonlinear properties resulting from space charge separation [10], and finally to anisotropic properties associated to local phase transition from the glass phase to anisotropic crystal phases [11,12].

Most of DLW studies have been performed in isotropic materials such as glasses [13], or isotropic crystals [14, 15]. However, several works have also been carried out in anisotropic crystals, in which waveguides have been written for laser amplification in the near-IR in Ti:Sa or Yb:KYW crystals [16, 17] and in the IR range at telecom wavelengths in the KGW crystal [18]. Waveguide writing is also reported for Raman gain in KGW crystal [18], for second-harmonic generation (SHG) in $LiNbO_3$ and BIBO [19, 20]. Such laser-written waveguides result from local modifications of the refractive index, either at the DLW focus (referred here as type I modification, showing non-permanent stability under heating [19]) or most likely around the DLW focus due to the induced photo-elastic stress field (referred here as type II modification, related to permanent laser-induced material structures above modification threshold) [19–21]. Waveguiding can result from various types of guiding structures such as single-line structure [22], with the inner part between a double-line structure [19], or even with a four-line structure to optimize SHG in BIBO waveguides [20]. Moreover, DLW of optical waveguides in anisotropic crystals appears to be dependent on the considered light propagation and polarization directions as well as the sample displacement direction [17, 19, 23], including non-reciprocal laser writing in non-centrosymmetric crystals such as $LiNbO_3$ [23]. The resulting waveguides show distinct behavior with respect to

#175917 - $15.00 USD Received 11 Sep 2012; revised 4 Nov 2012; accepted 4 Nov 2012; published 8 Jan 2013

transverse electric or magnetic modes for both guiding and amplification [18, 20]. Moreover, waveguide DLW has already been demonstrated in a large variety of crystals from the uniaxial optical class [19, 22–25] and from the biaxial optical class including monoclinic crystals [17, 18, 20]. These demonstrations included cases of propagation directions out of the principal axes of the dielectric frame where spatial walk-off takes place. However, the anisotropy of multi-photon processes that occur during DLW is almost never discussed in detail, especially for propagation out of the dielectric axes. Besides, in monoclinic crystals, resonant linear absorption and fluorescence properties were recently reported to show principal directions that differ from the well-known dielectric axes [26–28]. Therefore, one might expect strong anisotropy for future multi-photon interactions for waveguide DLW, where optimal crystal orientations and laser polarization are still to be determined.

From an instrumental point of view, laser-written waveguide structures have been observed by using a wide range of imaging techniques, such as transmission electron microscopy (TEM) [21], polarization microscopy [14, 23], atomic force microscopy (AFM) [14], and confocal Raman imaging [25]. Therefore, two-photon excited fluorescence is expected to be of particular interest to probe optical anisotropies of both pristine and structured crystals, since such technique can be controlled below laser-induced crystal modification. Two-photon fluorescence could thus provide further relevant tool for 3D local probing with laser/crystal interactions in polarized light.

In this article, we consider the nonlinear two-photon absorption and the subsequent fluorescence emission, both in polarized light, in the monoclinic biaxial borate crystal $Li_6Y(BO_3)_3$, doped with the Eu^{3+} rare earth ion. The reported work is performed below laser-induced crystal modification threshold, and it provides thus a preliminary work towards potential DLW of waveguides in such crystal. Thanks to spatial walk-off for propagation out of the dielectric axes, we report on single-beam dual-voxel nonlinear excitation of fluorescence, as well as its polarization analysis. The voxel spatial locations and the collected fluorescence intensity are compared for each pump and fluorescence polarization schemes. When considered above the laser-induced permanent modification threshold, such multi-photon excitation may further lead to original single-beam dual-voxel DLW, which might open the ability to simultaneously write two parallel optical waveguides, as highly considered by *Burghoff et al.* [19]. In a reversed approach, these developments also introduce the same potentialities for further single-beam dual-voxel laser probing. Finally, these aspects contribute to develop nonlinear local probing techniques in crystals with two-photon excited fluorescence in polarized light, so as to optically measure local inhomogeneities in laser materials, these modifications resulting either from undesired laser damage or from controlled DLW.

2. $LiY(BO_3)_3:Eu^{3+}$ crystal orientation

The considered crystal was a lithium yttrium borate crystal matrix, labeled $Li_6Y(BO_3)_3$, grown with the Chockralzki technique under congruent melting, with a 26% atomic substitution of Y^{3+} ions by Eu^{3+} ions, providing additional spectroscopic properties without significant changes of the initial crystal matrix properties [29, 30].

The $Li_6Y(BO_3)_3:Eu^{3+}$ biaxial crystal, hereafter labeled LYB:Eu, is a centro-symmetric crystal that belongs to the {P 2_1/c} symmetry group (crystallographic data on isostructural Yb matrix available in ref. 31). Its crystallographic frame (a, b, c) is a non-orthogonal frame where a = 7.157 nm, b = 16.378 nm, and c = 6.623 nm; The monoclinic axis b is perpendicular to the (a, c) plane; the angle β = (a, c) is typically 105.32°. Strong anisotropy of its optical properties is expected due to the monodimensional connexion of the rare earth polyhedra forming chain parallel to the c-axis. The orthonormal dielectric frame (X, Y, Z) is partially attached to the crystallographic frame, since symmetry considerations impose the Y and b vectors to be collinear. Note here that the dielectric Y-axis is therefore strictly fixed by crystallographic properties, while the (X, Z) vectors remain unfixed with an *a priori* possible

#175917 - $15.00 USD Received 11 Sep 2012; revised 4 Nov 2012; accepted 4 Nov 2012; published 8 Jan 2013

dispersion of orientation with wavelength [32, 33]. The four vectors (X, Z) and (a, c) are therefore all distinct but they are contained in the same plane, in relation to the typical dielectric orientations, with (a, X) = 39° and (c, Z) = 24° [34], as seen in Fig. 1(a).

The LYB:Eu sample under study was oriented by X-ray diffraction, cut with a 1 mm thickness and polished to optical quality with faces perpendicular to the crystallographic c-axis, ensuring the fixed dielectric b-axis to be parallel to the polished faces, as illustrated in Fig. 1(b). For such light propagation direction along the c-axis that belongs to the (X, Z) dielectric plane, the two polarization eigenmodes are orthogonal to each other. The first polarization mode, labelled as the ordinary mode $\overrightarrow{e_o} = \{0,1,0\}$ in Cartesian coordinates in the dielectric frame, is parallel to the b-axis, while the second mode, labelled as the extraordinary mode $\overrightarrow{e_e} = \{-\cos(\theta-\rho),0,\sin(\theta-\rho)\}$ is perpendicular to the b-axis, and thus tangent to the (a, c) plane. The angle θ is the spherical angle in the (X, Z) dielectric plane that depicts the selected propagation direction, here along the c-axis so that $\theta = (Z,c)$, while the angle ρ is the associated double refraction angle [35]. The ordinary mode orientation is fixed by crystallographic symmetry, while the extraordinary mode orientation might *a priori* disperse with wavelength in such monoclinic system [32, 33]. Therefore, note that this crystal orientation has been selected on purpose, since such orientation affords to independently address each polarization eigenmode, for both excitation and collection of fluorescence, without being sensitive to any dielectric frame dispersion. One can thus ensure to perform excitation and emission measurements along one single emission polarization mode at a time, which was a necessary precaution for the two-photon fluorescence analysis in polarized light described hereafter.

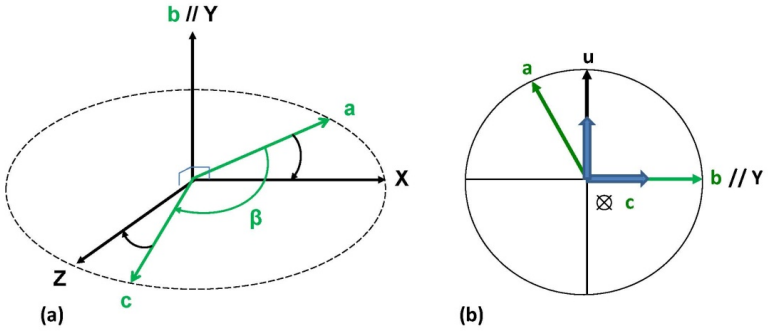

Fig. 1. (a) Relative orientation of the crystallographic frame (a, b, c) and the partially attached dielectric frame (X, Y, Z) in the LYB:Eu monoclinic crystal. (b) LYB:Eu crystal sample orientation under microscope experiments with light propagation direction along the c-axis, associated to two polarization eigenmodes respectively parallel or perpendicular to the b-axis, thus respectively parallel to the Y-axis or to the u-direction; blue arrows indicate the polarization directions of the experimental setup described in Fig. 2, ensuring the relevant correspondence of both the crystal polarization eigenmodes and the experimental detection directions in polarized light.

3. Experimental setup

The experimental setup was based on a home-made nonlinear fluorescence microscope, including a femtosecond laser (Ti:Sa oscillator, 2W, 80 MHz, 120 fs at 800 nm, Tsunami, Spectra Physics), an acousto-optic modulator and a half wave plate at 800 nm to control both the incident irradiance and laser polarization, a microscope objective (Mitutoyo, APO PLAN, 100 × , NA 0.9), and a high precision 3D translation stage for nanometric positioning of the crystal under irradiation (XMS-50 stages, Micro-Contrôle, 50 nm resolution). Two-photon excited fluorescence was obtained by soliciting the 4f-4f atomic transitions of the europium ions. Indeed, two-photon excited fluorescence (absorption in the $^5L_6$ excited level of Eu^{3+} and

#175917 - $15.00 USD Received 11 Sep 2012; revised 4 Nov 2012; accepted 4 Nov 2012; published 8 Jan 2013

emission from the $^5D_0$ singlet down to the ^7F_J (J = 0-6) manifold at around 613 nm) was detected in epi-collection configuration in polarized light, with light propagation also along the c-axis, with a CCD camera (Sony XCD-SX90CR). Since the energy difference between the $^7F_0$ ground and $^5L_6$ excited levels typically corresponds to 3.16 eV (394.5 nm) [30], the simultaneous absorption of two photons from the incident broadband laser beam at 800 nm matches rather well such energy difference, leading to an almost optimal resonant two-photon absorption. The $^5L_6$ excited level undergoes fast non-radiative multiple de-excitations towards the lower excited level $^5D_0$ which energy position is typically located at 2.15 eV (580 nm) from the $^7F_0$ ground level. Such $^5D_0$ excited state is known to show long-lasting fluorescence emission, with a millisecond-scale lifetime, towards the ^7F_J (J = 0-6) ground manifolds, especially through the strong emission transition of 2.03 eV (613.5 nm) towards $^7F_2$ in the case of highly Eu^{3+}-doped LYB matrix [30].

The fluorescence was recorded by the CCD camera without spectral discrimination, leading to the spectral integration of fluorescence from the $^5D_0 \rightarrow {}^7F_J$ emission levels in the orange-red range between 580 nm and 750 nm, with a maximum emission around 613 nm. The low spectral dispersion of the refractive index properties of this material in the orange-red-NIR range led the different emission lines to undergo the same propagation behavior. Finally, this setup, as seen in Fig. 2, authorized to independently control the incident beam polarization and that of the epi-collected fluorescence emission. The Glan polarizer was alternatively aligned along each of the two polarization eigenmodes of the epi-collected fluorescence.

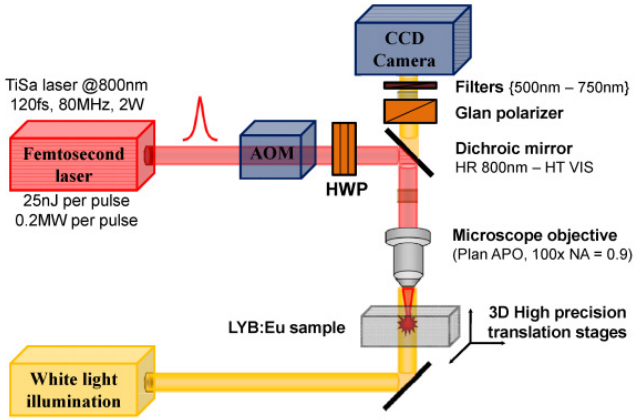

Fig. 2. Experimental setup of the homemade femtosecond nonlinear microscope, providing independent control of the irradiating beam polarization with the half wave plate (HWP) orientation and of the selected polarization of the fluorescence emission with the Glan polarizer.

4. Linear propagation along the c-axis and walk-off aspects

The crystal orientation, along the c-axis, imposed the extraordinary polarizations to undergo the double refraction effect with a spatial walk-off angle between the extraordinary wave vector $\overrightarrow{k_e}$ and the associated extraordinary Poynting vector $\overrightarrow{\pi_e}$ related to energy propagation. On the other hand, the ordinary wave vector $\overrightarrow{k_o}$ and Poynting Vector $\overrightarrow{\pi_o}$ were collinear to each other (as what classically happens with DLW in isotropic materials). Thanks to the polarization discrimination of both the two-photon excitation beam and the epi-collected fluorescence, these ordinary/extraordinary vectors were distinctly observed for both the pump and the fluorescence beams. Irradiation focusing was typically performed at 320 µm below the crystal surface, ensuring linear propagation over sufficient distance to spatially separate the ordinary and extraordinary polarizations.

#175917 - $15.00 USD Received 11 Sep 2012; revised 4 Nov 2012; accepted 4 Nov 2012; published 8 Jan 2013

With the excitation beam being polarized at 45° with respect to the b-axis and the u-direction, both ordinary and extraordinary propagation modes were simultaneously injected in the LYB:Eu sample, leading thanks to walk-off aspects to two distinct nonlinear two-photon excitations at the two spatially separated nonlinear voxels, as illustrated in Fig. 3(a). For irradiation below laser-induced permanent modification threshold, each nonlinear voxel then behaved as a distinct and independent fluorescence emission point, each one simultaneously providing ordinary and extraordinary polarized fluorescence emissions, as illustrated in Figs. 3(c) and 3(d), respectively. Note that the microscope objective imposed the angular selection of the epi-collected fluorescence wave vectors for both ordinary and extraordinary polarization modes, from each of the two nonlinear excited voxels, which insured the spatial discrimination of the distinct fluorescence spots in the CCD images, as illustrated in Fig. 3(c) and 3(d) and as further demonstrated in Fig. 4. For hypothetic irradiation above laser-induced permanent modification threshold, Fig. 3(b) reminds the illustration of a hypothetical refractive index increase around laser-induced structures, due to photo-elastic stress-induced field, in the potential case of type II waveguide writing where the guiding area may stand in the inner part between the two laser-induced structured lines, as proposed by Ref [19]. Such type II material modification has yet not been reported in this LYB:Eu crystal. However, for irradiances above permanent material modification threshold in the case of our single-beam dual-voxel irradiation, one might expect to simultaneously generate the two modified lines, instead of two successive writing steps in the current approach. Such single-beam dual-focus waveguide writing is thus a new open perspective.

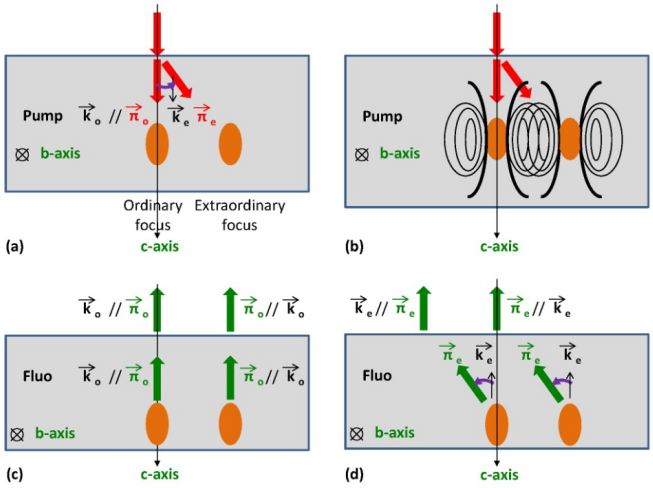

Fig. 3. (a) Illustration of the two nonlinear voxels resulting from the pump focusing of each polarization mode, where the extraordinary mode undergoes spatial walk-off leading spatial separation of the Poynting vectors; (b) Schematic field of hypothetical stress-induced refractive index increase from single-beam dual-voxel irradiation above permanent modification irradiance threshold, potentially leading to the simultaneous writing of two structured areas at the root of type II waveguiding in their inner region, as developed in Ref [19]; (c) & (d) Illustrations of the fluorescence propagation emitted from each of the nonlinear voxels below permanent modification thresholds, for both ordinary and extraordinary polarization modes and epi-collection propagation.

Each nonlinear voxel had true physical existence and location since it corresponds to where energy was locally deposed inside the crystal. However, from each nonlinear voxel, two distinct fluorescence polarization modes led to two distinct images at different spatial positions, even if these images were emitted from the same voxel. Each polarization scheme is separately presented in Fig. 4, demonstrating here the ability to spatially discriminate each case. Figures 4(a), 4(b), 4(c) and 4(d) report on the four polarization schemes for both the

#175917 - $15.00 USD Received 11 Sep 2012; revised 4 Nov 2012; accepted 4 Nov 2012; published 8 Jan 2013

pump and epi-collected beams with ordinary/ordinary, ordinary/extraordinary, extraordinary/extraordinary and extraordinary/ordinary polarization orientations, respectively. The three spatial positions of the four spots were spatially separated in the direction perpendicular to the b-axis, thus in the (Z, X) plane where double refraction takes place for the propagation along the c-axis. Moreover, Fig. 4 reveals distinct spatial shapes for each imaged spot, with a very circular transverse section for the ordinary/ordinary polarization scheme while the ordinary/extraordinary one showed a cross-like transverse section. These specific aspects of fluorescence images result from distinct imaging conditions, related to distinct solicitations of the refractive index surface in polarized light in the monoclinic crystal. Still, these images were remarkably spatially defined although, due to its large numerical aperture, the microscope objective integrated a large angular distribution of wave vectors surrounding the c-axis direction in the crystal, for each polarization configuration.

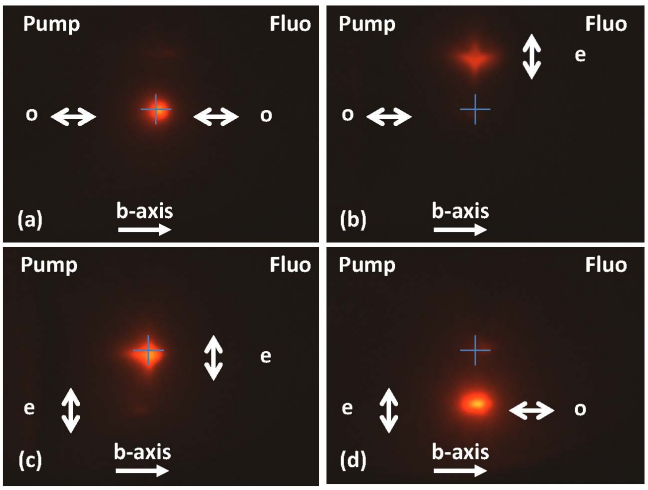

Fig. 4. Pictures of the two-photon excited epi-fluorescence in polarized light for both the pump laser beam and the collected beam. Polarizations o and e stand for the ordinary and extraordinary modes, respectively, for both the pump and the epi-fluorescence beams. (a), (b), (c) and (d): Polarization schemes with oo, oe, ee and eo polarization modes for the pump and the epi-fluorescence beams, respectively. The cross is at the same place in each picture, and is present for visual help.

The three fluorescence positions from the four polarization schemes, reported in Fig. 4, confirmed the understanding of the linear propagation of both the exciting and fluorescence beams, as illustrated in Fig. 3. It also demonstrated that the double refraction angle was very similar for these two beams with quite similar wavelengths. This similarity between the double refraction angles corresponds to a very limited refractive index dispersion between the 800 nm pump beam and the typically 600 nm fluorescence beam. It also tends to indicate an almost null orientation dispersion of the dielectric frame for wavelengths between 600 nm and 800 nm. Moreover, the extraordinary/extraordinary polarization scheme, where both the exciting and the epi-fluorescence beams undergo double refraction, was imaged at the same camera position as the ordinary/ordinary polarization scheme, since walk-off effects cancel, due to the fact that the two beams propagated along the same c-axis but in opposite directions (as it is sometimes exploited in OPO cavities with two twin crystals in opposite orientations to cancel double refraction effects [35]). Such absence of orientation dispersion of the dielectric frame with respect to the crystallographic one was also reported elsewhere, in the case of the monoclinic crystals YCOB and YCOB:Nd [36], contrary to the case of BIBO [33].

#175917 - $15.00 USD Received 11 Sep 2012; revised 4 Nov 2012; accepted 4 Nov 2012; published 8 Jan 2013

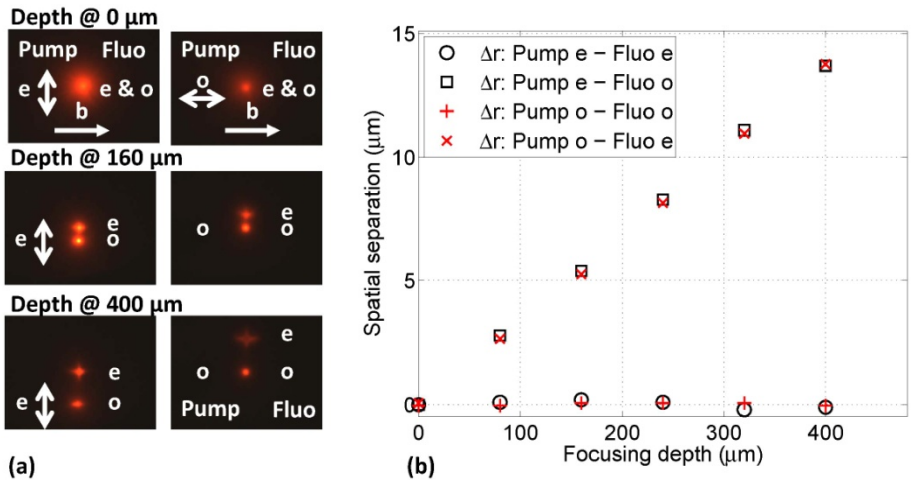

Fig. 5. (a) Distinct fluorescence spots for each pump polarization mode, for different optical focusing depths under the crystal surface. (b) Walk-off spatial separation corresponding to the distance between the centres of the ordinary and extraordinary polarized fluorescence spots for a given two-photon excited voxel, versus the focusing depth for each of the four propagation schemes.

The spatial separation of the extraordinary polarization modes were studied with respect to the focusing depth for both the pump beam and the subsequent epi-collected fluorescence in polarized light. The optical focusing depth was estimated as the mechanical vertical translation of the sample times the typical refractive index value of 1.6 [37]. As the optical focusing depth increased, the walk-off separation increased, starting from zero when the pump was focused at the crystal surface to tens of microns when the pump was focused well below the surface, as seen in Fig. 5(a). Figure 5(b) reports on the spatial displacement of the fluorescence spots related to each of the four possible polarization schemes, where the slope of the e-o and o-e polarization schemes directly corresponds to the solicited double refraction angle. Here, such slope typically leads here to a 2° double refraction angle, which is standard in the case of monoclinic borate crystals in the (X, Z) plane [38]. The effective position of ordinary/ordinary polarization scheme was invariant with the focusing depth, as well as the extraordinary/extraordinary one where the walk-off translation for the pump and epi-collected beams appeared to compensate each other, leading to the same effective spot position as that of the ordinary/ordinary scheme. For polarization schemes where only one extraordinary polarization was present for either the pump or the epi-collected fluorescence, the spatial displacement was the same, following a standard linear law with the propagation distance inside the crystal corresponding to the imposed depth of linear focusing. Despite the tight focusing under microscope objective (NA = 0.9) and high peak irradiances, such linear dependence confirmed the linear behavior of both the pump and the fluorescence propagations, despite the nonlinear behaviour of the two-photon excitation process of the fluorescence emission, as demonstrated below in section 5.

5. Two-photon excited fluorescence

The reported fluorescence spots resulted from two-photon excitation and subsequent single-photon spontaneous emission, which is insured by the set of filters in front of the camera leading to a band-pass collection between 500 nm and 750 nm. The fluorescence intensity was studied with respect to the incident pump irradiance, for the four polarization schemes. The expected quadratic fluorescence intensity dependence with the injected pump irradiance was observed and fitted, for incident powers typically below 400 mW. We remind here that no second-order nonlinear process can take place here since such material response is null due

#175917 - $15.00 USD Received 11 Sep 2012; revised 4 Nov 2012; accepted 4 Nov 2012; published 8 Jan 2013

to its centro-symmetry. Moreover, the reported phenomena correspond to two-photon absorption (which is related the imaginary part of the third-order nonlinearity, which means a four-wave interaction), followed by non-radiative energy transfer, finally followed by single-photon fluorescence emission (which is related the imaginary part of the first-order optical response, i.e. the linear response, which means a two-wave interaction) [39]. Note that the epi-collection experimental setup mostly forbids to consider any four-wave interaction where two incident pump photons would coherently lead to the weakly-efficient parametric emission of two distinct photons at new wavelengths, since such process would mostly impose forward parametric fluorescence emission (with a not necessarily collinear scheme). Additionally, the fluorescence emission spectrum was checked in the visible red-orange range, and it directly corresponded to the classical single-photon exited fluorescence emission of Eu^{3+} ions in the crystal matrix as reported in [30], which confirms the overall scheme of two-photon nonlinear excitation followed by single-photon linear emission.

For the estimation of the related pump irradiances, we took into account both the Fresnel losses at the input surface of the illuminated crystal, as well as the temporal broadening of the 120 fs Fourier-limited pulses to the typically estimated 230 fs chirped pulse resulting from propagation through the experimental setup. In the case of diffraction-limited tight focusing where $\omega_p \sim 0.61\lambda / NA \sim 0.55\ \mu m$, input powers of 400 mW typically correspond to 2 $TW.cm^{-2}$ irradiances in our experimental case. Note however that such temporal broadening is the same whatever the considered polarization scheme, so that the reported anisotropies are consistent one with another. Each experimental series was fitted with the same quadratic model $A_{ij} + B_{ij}.I^2$, where indices *i* and *j* stand for the considered ordinary or extraordinary polarization mode, respectively for the incident pump beam and the collected fluorescence beam. Since two-photon excited fluorescence was recorded in arbitrary units, the A_{ij} parameters depict the experimental background while the B_{ij} are proportional to the cross-sections of two-photon excited fluorescence emission in polarized light. Therefore, only the ratios of the B_{ij} parameters provide information about the anisotropies of the solicited optical properties of the LYB:Eu crystal. Indeed, the fitting parameters for quadratic dependence typically showed that the angular-averaged cross-section of the epi-collected fluorescence emission along the c-axis is quite similar for the ordinary and extraordinary polarizations (less than 10% difference since B_{oo}/B_{oe} ~1.07 and B_{eo}/B_{ee} ~1.03). Such similarity in the considered fluorescence emission cross-sections is shown in Fig. 6, where slopes with the same pump polarization are almost overlapped for the two fluorescence emission polarizations. However, it is remarkable to note that the solicited two-photon absorption is typically twice larger for the extraordinary pump polarization than the ordinary one, since B_{eo}/B_{oo} ~1.95 and B_{ee}/B_{oe} ~2.03. Here also, Fig. 6 shows the clear distinction between slopes with the same fluorescence emission polarization, but with distinct pump polarization. Such anisotropy should highly be considered for further single-beam dual-voxel DLW of waveguides, where a balanced amount of the incident power should simultaneously be injected in each of the two voxels. Indeed, one should thus properly balance the injected power in each voxel by optimizing the orientation of the incident pump polarization between the ordinary and extraordinary polarization modes, so as to potentially perform relevant double-lines structures for light guiding in their inner part. Moreover, the continuous rotation of the incident pump polarization should provide additional information on the complete description of the fundamental process at play, as experimentally considered elsewhere [40].

#175917 - $15.00 USD Received 11 Sep 2012; revised 4 Nov 2012; accepted 4 Nov 2012; published 8 Jan 2013

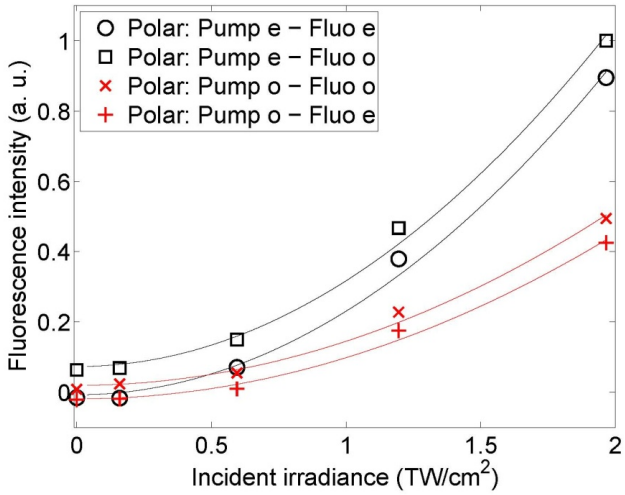

Fig. 6. Fluorescence emission irradiances in polarized light, depending on the incident pump irradiance along the c-axis propagation direction, for the four ordinary/extraordinary polarization schemes of the pump and fluorescence beams. Fitted model $A + B.I^2$ (full lines) for each polarization scheme. The optical focusing depth was 320 µm below the crystal surface.

6. Conclusion & perspectives

In this article, we report on the two-photon excited fluorescence emission in the LYB:Eu monoclinic crystal, under tight focusing of a near-IR femtosecond laser beam. We have demonstrated the creation of two separate nonlinear voxels associated to the two pump polarization eigenmodes, these voxels leading to light emission in the two fluorescence polarization eigenmodes along the epi-collected signal. Spatial walk-off propagation leads to the spatial discrimination of each of the four polarization schemes, for both the pump and the fluorescence beams, in such biaxial crystal oriented along the crystallographic c-axis. The third-order nonlinear behavior of the two-photon absorption process was demonstrated with the quadratic evolution of the fluorescence emission versus the pump irradiance, showing anisotropic polarization dependence. A remarkably large polarization dependence has been demonstrated, where the extraordinary pump polarization provides twice more fluorescence excitation than its ordinary counterpart in the considered experimental conditions, suggesting the subsequent anisotropy of laser-induced modification thresholds for higher incident irradiances. The reported observations rise further fundamental questions as the complete description of the angular distribution in polarized light of the two-photon absorption behavior. Such issue requires a future experimental analysis including the continuous rotation of the pump polarization [40], as well as the consideration of several crystal orientation and light propagation directions. Such issue would also extend recent advances in monoclinic bulk crystals where angular distributions in polarized light of both fluorescence emission and single-photon absorption have been experimentally and theoretically explored, leading to very specific optical behavior [41].

The reported observations have been obtained below laser modification thresholds for the considered crystal, under microscope objective focusing corresponding to diffraction-limited spatial resolution. These results open interesting experimental capabilities of micron-scale 3D local probing of crystal homogeneity with a near-IR femtosecond laser beam. Such probing could be obtained either from a single excited voxel or with differential measurements from the two nonlinear voxels when simultaneously activated with a polarization control. Such probing could thus enable the local characterization of DLW, potentially doubling the speed of data reading due to single-beam dual-voxel probing, in information storage applications. In

#175917 - $15.00 USD Received 11 Sep 2012; revised 4 Nov 2012; accepted 4 Nov 2012; published 8 Jan 2013

the case of the potential laser crystal LYB:Eu [42], such a two-photon fluorescence technique could help for the observation of material ageing in order to anticipate any optical breakdown.

Finally, the reported observations should be extrapolated above laser-induced permanent modification thresholds for the considered crystal, so as to provide single-beam dual-voxel DLW, leading to the simultaneous writing of photo-modified regions. By adjusting the depth of focusing, the distance between the two regions could be controlled, which open interesting potentials for the simultaneous writing of type II waveguides [19]. The reported anisotropy of the nonlinear fluorescence excitation imposes a careful balance of the deposited dose in each voxel. Finally, such dual-voxel DLW could apply for double-line laser or nonlinear waveguides in bulk crystals, as well as for nonlinear waveguides in periodically poled crystals where the considered light propagation direction can also be non perpendicular to the periodic ferroelectric domain walls [43, 44].

Acknowledgments

This work was supported by the French Agency of National Research and the French Aquitaine region.

#175917 - $15.00 USD Received 11 Sep 2012; revised 4 Nov 2012; accepted 4 Nov 2012; published 8 Jan 2013